PROCEEDINGS OF SCIENCE

Polarized Photocathode R&D at BNL and spin consideration for the EIC preinjector

Jyoti Biswas,[a,*] **Erdong Wang,**[a] **Omer Rahman,**[a] **John Skaritka,**[a] **Adam Masters,**[b] **Sylvain Marsillac**[b] **and Tai-De Li**[c]

[a] *Brookhaven National Laboratory, Upton, NY 11973, USA*
[b] *Old Dominion University, Norfolk, VA 23529, USA*
[c] *City University of New York, New York, NY 10017, USA*

E-mail: jbiswas@bnl.gov, wange@bnl.gov

Superlattice GaAs photocathodes are vital for producing polarized electron beams for the Electron-Ion Collider (EIC) at Brookhaven National Laboratory. The electron pre-injector at the EIC requires a 7 nC bunch with at least 85% spin polarization from a GaAs-based superlattice cathode. The doping density of the surface layer of the cathode needs to be optimized to extract a high bunch charge beam from the high-voltage DC gun. The polarization axis of the emitted beam is longitudinal, and it will be rotated to transverse direction using two Wien filters, each rotating the spin by 45 degrees. In this paper, we report our progress in recent R&D efforts for polarized photocathodes, and spin considerations for the EIC.

20th International Workshop on Polarized Sources, Targets, and Polarimetry (PSTP 2024)
September 22-27, 2024
Jefferson Lab, Newport News, VA, USA

*Speaker

PoS(PSTP2024)026

1. Introduction

Polarized electron sources play a crucial role in various fields of fundamental research, including condensed matter physics and elementary particle physics. Key accelerator facilities such as the Continuous Electron Beam Accelerator Facility (CEBAF) at Jefferson National Laboratory(JLab)[7] and the Electron-Ion Collider (EIC) at Brookhaven National Laboratory(BNL)[8] require polarized electron beam. Polarized positron beams can be generated from polarized electron beams by impinging on a high-Z-target material[12].

Bulk GaAs can achieve a maximum polarization of 35–40% due to heavy-hole and light-hole degeneracy in the $2p_{3/2}$ state and spin relaxation. Strained GaAs/GaAsP-based superlattice breaks this degeneracy, enabling spin-polarized electrons from a single band. Although a spin polarization of approximately 92% has been achieved, the quantum efficiency (QE) mostly remains around 1% or lower at near-bandgap photon energies[1, 2]. Adding a Distributed Bragg Reflector (DBR) under the superlattice layer enhances photon absorption and improves QE. This design previously achieved 84% electron spin polarization (ESP) and 6.4% QE at 776 nm laser wavelength[3].

The Electron-Ion Collider requires a polarized electron beam with an initial bunch charge of 7 nC and a minimum electron spin polarization (ESP) of 85% from the source. This work presents the research and development (R&D) efforts on polarized photocathodes, as well as the implementation of Wien filter spin rotators to manipulate electron spin orientation from longitudinal to vertical.

2. Polarized Photocathode R&D at BNL

The limited availability of GaAs/GaAsP superlattice photocathodes has resulted in a global "spin crisis", with no vendors currently capable of providing photocathodes that simultaneously achieve high QE and ESP. This challenge has prompted extensive collaborative efforts worldwide, involving institutions such as Old Dominion University, JLab, Sandia National Laboratories, and others, to revive the development of high-QE and high-ESP photocathodes.

There are two main methods to grow high-polarization GaAs/GaAsP photocathodes: Molecular Beam Epitaxy (MBE) and Metal Organic Chemical Vapor Deposition (MOCVD). The critical factor in MBE is the deposition rate, typically less than 3,000 nm per hour, facilitating the epitaxial growth of the films. In contrast, MOCVD systems are relatively inexpensive and the growth can be tweaked many times before achieving both good QE and ESP. The superlattice GaAs/GaAsP discussed throughout this paper is grown in a MOCVD system at the Rochester Institute of Technology by co-authors from Old Dominion University. The details of the growth procedure are discussed elsewhere[4].

2.1 Optimize pre-cleaning and heat treatment

GaAs/GaAsP-based superlattice photocathodes grown using the MBE system are usually terminated with an arsenic capping layer to prevent contamination at the surface. The arsenic capping layer can be easily removed in an ultra-high vacuum (UHV) system with a heat cleaning temperature of 450°C or higher. In a MOCVD system, it is rather challenging to incorporate an arsenic capping layer. As a result, GaAs when exposed to air during handling and installation, can create a thin oxide layer. In general, both Ga and As oxides form as a result of exposure to air. Heat treatment

of around 580°C in UHV usually completely eliminates all oxides from the surface. However, heat treatment at higher temperature (i.e., at ~ 580°C) may cause interlayer material diffusion, which could cause loss of surface dopant, and hence increase in the surface charge effect during operation in high-voltage DC gun.

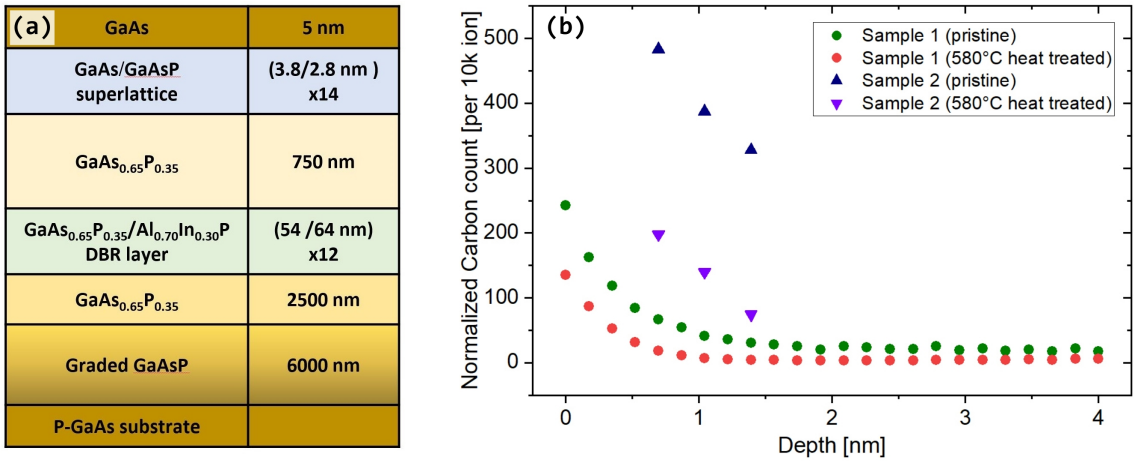

Figure 1: (a) Schematic structure of the superlattice GaAs/GaAsP photocathode with DBR layer. (b) SIMS cross-sectional profile for pristine sample, and sample from the same wafer after it went through two heat cleaning cycles at 580°C. Both for samples 1 and 2, we observed a reduction of carbon count in the surface layer[5].

A schematic drawing of the structure of the SL-DBR photocathode is shown in Fig.1(a). The sample under discussion in this paper is doped with carbon in the surface layer, and the rest of the GaAs/GaAsP layers are doped with zinc. The top 5 nm is p-doped with carbon with a carrier concentration of around $5\times10^{19}/cm^3$. We wanted to verify if high-temperature heat treatment such as 580°C could cause any reduction in doping density at the surface layer. Transmission electron microscopy (TEM) is not very suitable for GaAs/GaAsP doping analysis since the density of GaAs is $4.5\times10^{22}/cm^3$ and high doping ($10^{19}/cm^3$) is only incorporated in the top 5 nm. To study doping density in the surface layer, we utilized secondary ion mass spectrometry (SIMS). Fig.1(b) shows carbon count per 10k total ion for both pristine sample and sample from the same wafer after 580°C heat treatment. To avoid background carbon count, we utilized a GaAs sample with no carbon doping as our sample for background correction. Fig.1(b) clearly shows that the high-temperature heat treatment of around 580°C has adverse effects on the surface doping density.

To reduce the heat cleaning temperature, we have incorporated a wet cleaning method before the sample installation into the vacuum system. We immersed the MOCVD-grown GaAs/GaAsP samples in a 36% purified hydrochloric acid solution for 45 seconds, dipped them in deionized water, blew them with high-purity dry N_2 for a few seconds, then promptly installed them in the cathode puck (with indium foil underneath for ohmic contact) and loaded them into the chamber through the load lock manipulator, and baked the manipulator section at 200°C for 72 hours. After the successful bake of the load-lock manipulator, the cathode puck was transferred into the preparation chamber. The base pressure of the preparation chamber was $\sim 1\times10^{-11}$ Torr. The sample went through two hours of heat treatment at around 450°C and slowly cooled down to room temperature.

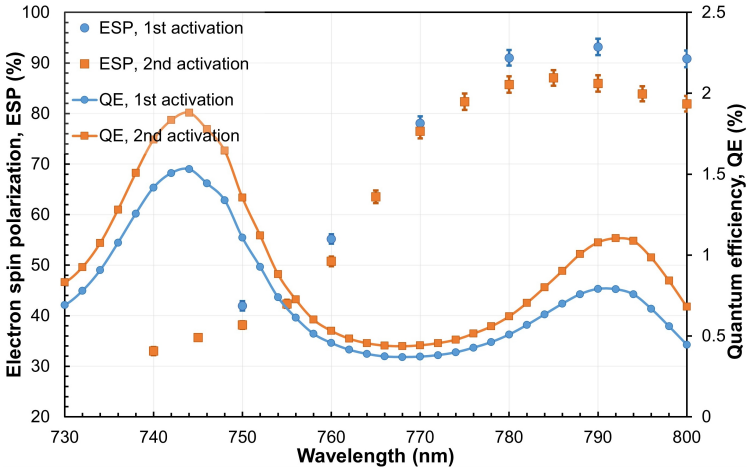

Figure 2: The QE and electron-spin polarization of MOCVD grown GaAs/GaAsP superlattice DBR photocathode as a function of the wavelength, measured at nearly identical location[5].

The sample was activated at room temperature in the Mott polarimeter preparation chamber to form a negative electron affinity (NEA) surface using the standard yo-yo activation procedure with Cs and O_2. A Superk EXTREME white-light source along with a monochromator alternative from NKT photonics was used to generate a single wavelength laser with tunability from 400 nm to 820 nm. Circularly polarized laser light was obtained by using linear film polarizer, quarter-wave plate, and polarizing beamsplitting cubes, all mounted at the top of the polarimeter and kept inside an enclosure. Details of the EIC Mott Polarimeter is discussed elsewhere[6].

The QE of the samples was scanned with a laser with a wavelength ranging from 720 nm to 800 nm. Fig.2 shows the spectral response and spin polarization of a superlattice DBR photocathode. At the center of the wafer, the peak QE wavelength position is close to the intended design value of approximately 780-785 nm. However, peak QE wavelength varies as we move from the center towards the edges of the wafer. Our study revealed a shift in peak QE wavelength from 770 nm to 790 nm across a 2-inch wafer, indicating nonuniformity in the DBR layer across the sample, likely due to nonuniform heating during the growth process in the MOCVD system.

In our current study, we have used a reduced heat treatment temperature of 450°C, which is sufficient enough to remove most of the arsenic oxides from the surface. Though high-temperature heat treatment of around 580°C is able to achieve a contamination-free surface and shows high QE[11], our motivation was to minimize the dopant diffusion at the surface layer so that high bunch charge could be extracted from the cathode in high voltage DC (HVDC) gun. We found that in terms of the achieved polarization from the SL-DBR cathode, there is no difference between 450°C and 580°C heat treatment.

2.2 Optimize surface doping and DBR pairs

The top 5 nm of the GaAs/GaAsP superlattice layer are usually terminated with highly p-doped material (i.e., zinc or carbon) so that it helps lower the work function, as well as prevent recombination of electrons and holes, making a net increase of emitted electrons from the cathode. Carbon was chosen as the dopant for the surface layer because (a) it has a relatively lower diffusion

rate compared to that of zinc and (b) because other superlattice layers are doped with zinc, doping the surface layer with carbon helps quantification through SIMS measurements.

To optimize the surface doping concentration, we tested four DBR superlattice GaAs samples with surface doping levels ranging from 1×10^{19} to 2×10^{20} $/cm^3$. The peak polarization starts to decline beyond $5 \times 10^{19}/cm^3$ due to the scattering of doping atoms with polarized electrons, leading to polarization degradation. Lower doping levels in general yield higher spin polarization, whereas higher surface doping helps suppress the surface charge effect while extracting an electron beam in an HVDC gun. Taking into account the merit figure ($P^2 \times QE$) of the polarized source, where P represents polarization, achieving high polarization is the most crucial factor. Therefore, based on this criterion, we determine to use the sample with the highest figure of merit, which has the optimal surface doping level of $5 \times 10^{19}/cm^3$.

A sample with an optimal surface doping of $5 \times 10^{19}/cm^3$ underwent pre-cleaning with HCL and a reduced heat treatment temperature of around 450°C in UHV. Subsequently, it was activated and tested in an HVDC electron gun[9]. The HVDC gun was operated at 300 kV, and the test of the SL-DBR cathode in the HVDC gun shows that a lower heat cleaning temperature of 450°C (compared with traditional 580°C heat treatment) helps to suppress the surface charge effect. Details of this study are discussed elsewhere[9].

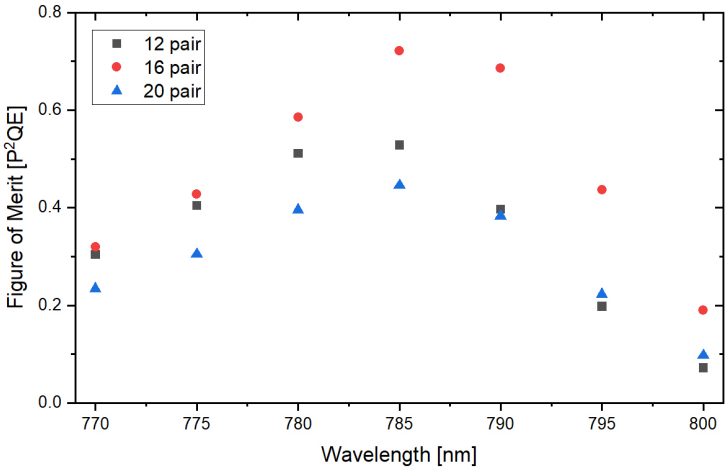

Figure 3: Figure of merit ($P^2 \times QE$) for superlattice DBR sample with a varied number of DBR pairs.

To optimize the number of DBR pairs, we have utilized samples with varied DBR pairs, ranging from 12, 16, and 20 pairs. The DBR pair is composed of alternate layer of $GaAs_{0.65}P_{0.35}$ and $In_{0.30}Al_{0.70}P$. The DBR pairs were Zn-doped with a doping density of $5 \times 10^{18}/cm^3$. The very surface carbon doping of all these samples was close to $5 \times 10^{19}/cm^3$. The main purpose of the DBR layer is to increase the absorption of photons in GaAs at a desired wavelength. However, having too many DBR layers could increase the cavity Q factor, causing a smaller bandwidth and a drop in QE. Fig. 3 shows a comparison of the figure of merit ($P^2 \times QE$) for different DBR pair numbers with respect to wavelength. A higher figure of merit was achieved for the sample with 16 DBR pairs.

3. Spin consideration for the EIC

The electron pre-injector at the EIC requires a 7.5 nC bunch with at least 85% electron spin polarization from the electron source. The spin direction from the GaAs photocathode is longitudinal, which will be rotated to vertical direction before injecting the beam into the ring. In the EIC CDR, we use the dipole-solenoid spin rotator at the end of the linac to rotate the spin[13]. However, the issues are: i)Needs specific energy; ii) CSR effects; iii) Not suitable at low energy (< 250 MeV) or very high energy like $3GeV$. Currently, we are considering using the Wien filter to do the spin rotation due to no significant limitations. Previously, the Wien filter operated only with beams below 200 keV and within tens of pC charge[14–16]. For the EIC beam of 320 keV, a longer length is required due to limitations in high-voltage feedthrough. However, this conflicts with the need for close placement of the focusing element to count high space charge. We are designing two Wien filters, each rotating the spin by 45°. Given the large beam size, a significant gap between the two electrical plates is necessary to maintain a uniform field and matched E-B fringe fields to minimize beam deflection. The design parameters for the high charge high energy Wien filter are shown in Table 1.

Table 1: Wien filter parameters

Parameter	**Value**
Charge [nC]	7
Energy [keV]	320
Length [m]	0.4592
Ey [MV/m]	1.44
Bx [G]	60.88
Rotating angle[degree]	45
Electrode gap [cm]	7
Feedthrough voltage [kV]	50.5

3.1 Wien filter design and generating Opera model and field profile

In Wien filter, the orthogonal electric and magnetic field is required to cancel out the deflecting force acting on the electron beam. At low energy, with $\beta = 0.788$ Wien filter can be an effective way to manipulate the spin of the electron beam. The spin rotation θ can be derived from Thomas BMT equation and simplified into the following:

$$\theta = \frac{eL}{m_0 c\beta\gamma^2}\left[\frac{E_y}{v_z}\right], \tag{1}$$

The net force on the beam is balanced by perpendicular E and B fields.

$$\vec{E_y} = -\vec{v_z} \times \vec{B_x} \tag{2}$$

Based on the above equation, the Wien filter parameters are calculated, keeping the large gap of 7 cm due to a large beam size. We kept a longer length of the Wien filter due to limitations of

the high voltage feedthrough. Though a shorter distance of the Wien is desired due to focusing, a longer length helps to use off-the-shelf feedthrough without much complications.

To shape the electric field in the fringe region, a Rogowski profile is employed at the end of the electrode plate. The electric and magnetic fields have different decay characteristics, so nickel plates are used to suppress the B-field in the fringe region, ensuring proper matching with the E-field in that region. Opera 3D electrostatic and magnetostatic solvers are used separately to simulate the electric and magnetic fields of the Wien filter. A perspective view of the Opera 3D model of the Wien filter is shown in Fig.4. 3D shaping of the iron core is used to better match the E-B field. Nickel plates on both sides of the Wien filter are used to shape the fringe B-field.

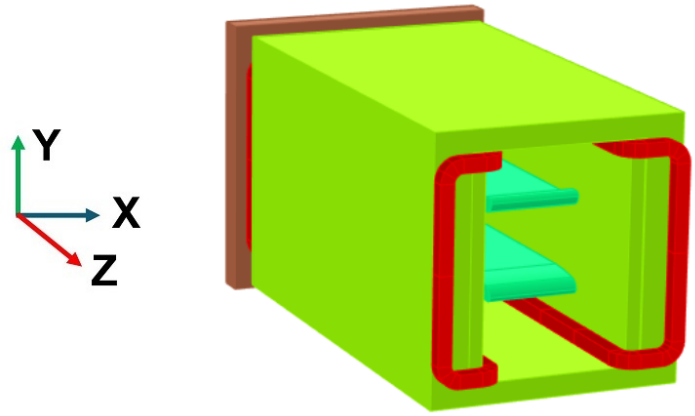

Figure 4: Perspective view of the Opera 3D model of the Wien filter. Nickel plates are used on both sides to shape the fringe B-field. The front-side Nickel plate is not shown here to make the electrodes visible.

Fig. 5 shows well-matched E_y and B_x components along the center line. The electrode plates' width and the transverse shaping of the iron core are optimized to achieve field matching not only along the center line but also in the transverse direction.

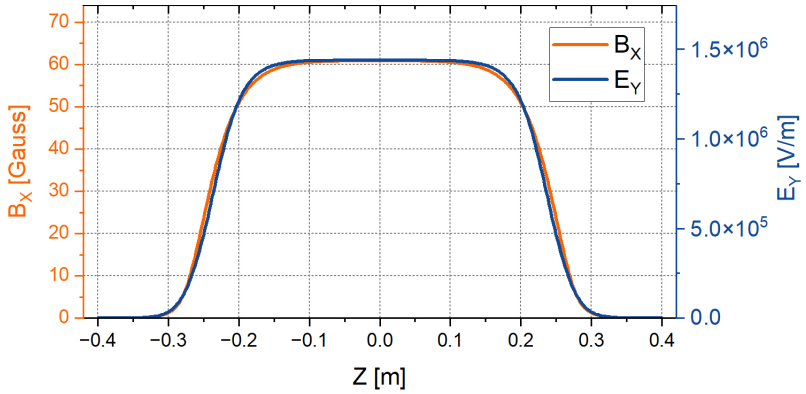

Figure 5: Simulated electric and magnetic field at the center-line generated from Opera 3D.

3.2 Beam dynamics through the Wien filter

Beam dynamics simulations with two Wien filters were carried out in Parmela and further checked with a General Particle Tracer (GPT). In Parmela, a 7.5 nC space charge-dominated beam

was generated from the 320 kV HVDC gun, with the gun electric field map imported from Poisson simulation software. The field profiles of the solenoid, thin quadrupole lenses, and Wien filters were used to transport the 7.5 nC space charge-dominated beam. Numerous optimization steps for the electrodes and magnets of the Wien filters were performed to minimize beam deflection in the Wien filter region. Fig. 6 shows the beam envelope of a 7.5 nC beam through Wien filter 1 and Wien filter 2. Quadrupole lenses in a triplet configuration were used before and between the Wien filters.

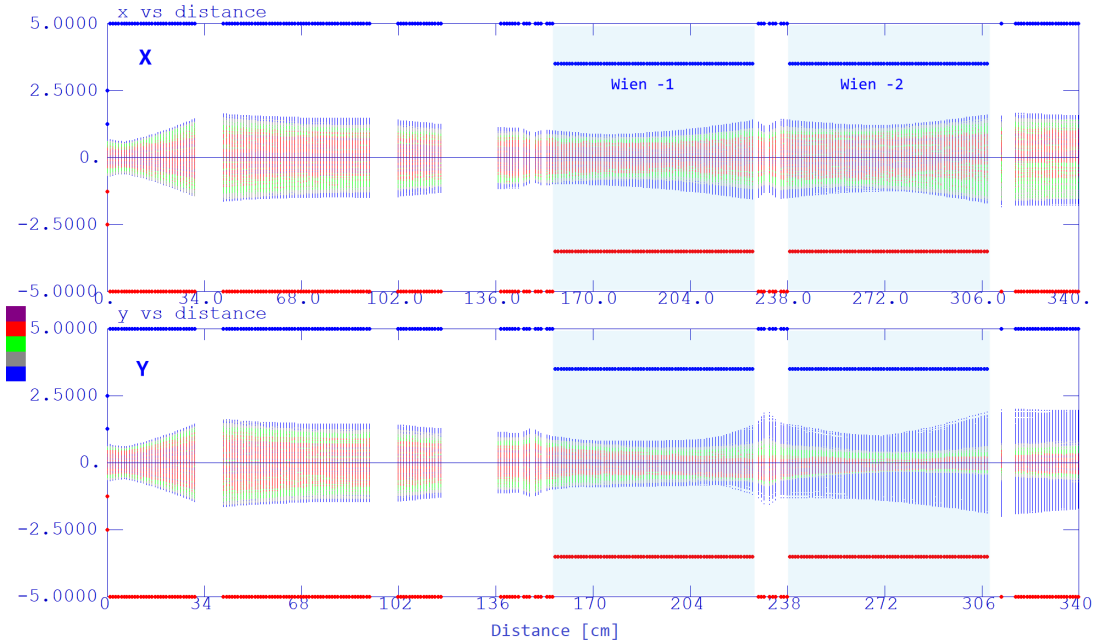

Figure 6: Simulated beam envelope of a 7.5 nC space charge-dominated beam through Wien filters 1 and 2, obtained using Parmela.

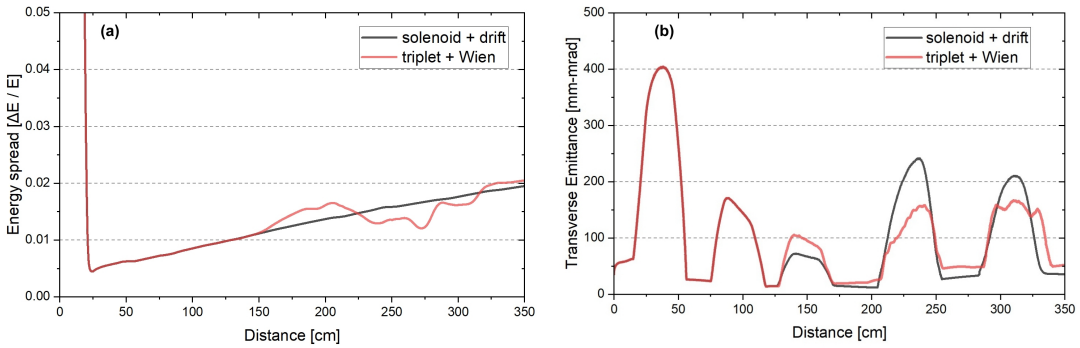

Figure 7: The evolution of (a) energy spread, and (b) normalized transverse emittance, with respect to distance from the cathode.

The evolution of energy spread ($\Delta E/E$) and transverse emittance with respect to distance are shown in Fig. 7. The bunch length of the beam from the cathode was 1.3 ns, bunch charge of 7.5 nC, and in beam simulation the space charge effect was considered. These simulations indicate that

a 7.5 nC beam can pass through both Wien filters. While there is a slight increase in emittance, it does not appear to significantly affect the overall performance. Although the EIC requirement specifies a 7 nC beam, a 7.5 nC beam was considered in the simulations to provide additional margin. Our analysis indicates that the high space charge from the beam has a negligible effect on the polarization degradation in the Wien filter.[10].

One of the challenging aspects of the Wien filter is constructing the electrode and magnet to meet the precise specifications required to maintain uniform electric and magnetic fields. Even a minor misalignment during commissioning or the bake-out process may affect the beam trajectories. Additionally, our analysis indicates that the combined ripple from the electrode high-voltage power supply and the magnet power supply needs to remain below 100 ppm. Therefore, developing a prototype is essential to validate this unique high-charge, high-energy Wien filter configuration.

4. Conclusion

In summary, we have optimized the pre-cleaning and heat treatment of MOCVD-grown GaAs/GaAsP superlattice photocathode that does not have any Arsenic capping layer. Before loading the sample into the UHV system, wet etching was carried out using HCl, and the heat treatment temperature was lowered to approximately 450°C to mitigate dopant diffusion caused by high temperatures. A mini Mott polarimeter was used to measure the optimal doping density in the surface layer, as well as the number of DBR pairs.

To manipulate spin direction from longitudinal to transverse, Wien filter configurations are studied. We have utilized Opera 3D to design the electrode and the magnet to match the transverse E-B field at the center as well as the fringe field region. Beam dynamics simulation shows a 7.5 nC beam can go through both the Wien filters, with non-significant emittance increase and energy spread.

Acknowledgments

Thanks to Matthew Poelker, Joe Grames, Carlos Hernandez-Garcia, and Gabriel Palacios-Serrano from Jefferson Laboratory for insightful discussion regarding the Wien filter. This work is supported by Brookhaven Science Associates, LLC under Contract No. DE-SC0012704 with the U.S. Department of Energy.

References

[1] Y. Mamaev *et al.*, "Optimized photocathode for spin-polarized electron sources", *Appl. Phys. Lett.*, 93, 081114 (2008); https://doi.org/10.1063/1.2976437

[2] X. Jin *et al.*, "High-Performance Spin-Polarized Photocathodes Using a GaAs/GaAsP Strain-Compensated Superlattice", *Appl. Phys. Expr.*, 06, 015801 (2012); https://doi.org/10.7567/APEX.6.015801.

[3] W. Liu *et al.*, "Record-level quantum efficiency from a high polarization strained GaAs/GaAsP superlattice photocathode with distributed Bragg reflector", *Appl. Phys. Lett.*, 109, 252104 (2016); https://doi.org/10.1063/1.4972180.

[4] B. Belfore *et al.*, "High figure of merit spin polarized electron sources grown via MOCVD", *Appl. Phys. Lett.*, 123, 222102 (2023); https://doi.org/10.1063/5.0170106

[5] J. Biswas *et al.*, "Quest for an optimal spin-polarized electron source for the Electron-Ion Collider", *IPAC2024*, Nashville, TN (2024); https://doi.org/10.18429/JACoW-IPAC2024-MOPR77.

[6] J. Biswas *et al.*, "Record quantum efficiency from strain compensated superlattice GaAs/GaAsP photocathode for spin polarized electron source", *AIP. Adv.*, 13, 085106 (2023); https://doi.org/10.1063/5.0159183.

[7] C. Leemann *et al.*, "The continuous electron beam accelerator facility: CEBAF at the Jefferson Laboratory", *Annual Review of Nuclear and Particle Science*, 51:413-450 (2001); https://doi.org/10.1146/annurev.nucl.51.101701.132327.

[8] C. Montag *et al.*, "The EIC Accelerator: Design Highlights and Project Status", *IPAC2024*, Nashville, TN (2024); https://doi.org/10.18429/JACoW-IPAC2024-MOPC67.

[9] E. Wang *et al.*, "High-intensity polarized electron gun featuring distributed Bragg reflector GaAs photocathode.", *Appl. Phys. Lett.*, 124 (25): 254101 (2024); https://doi.org/10.1063/5.0216694.

[10] E. Wang, "Space Charge Effects on Spin Polarization in High-Intensity Preinjector", *BNL-226378-2024-TECH*; https://doi.org/10.2172/2478783

[11] J. Biswas *et al.*, "Revisiting heat treatment and surface activation of GaAs photocathodes: In situ studies using scanning tunneling microscopy and photoelectron spectroscopy", *J. Appl. Phys.*, 128, 045308 (2021); https://doi.org/10.1063/5.0008969.

[12] J. Dumas *et al.*, "Polarized Positrons at Jefferson Lab", *AIP Conf. Proc.*, 1149, 1184–1188 (2009); https://doi.org/10.1063/1.3215617.

[13] N. Tsoupas *et al.*, "The eRHIC spin rotator and the beam optics of the 400 MeV transfer line to RCS", *International Journal of Modern Physics A* , Vol. 34, No. 36 (2019) 1942014 (2019); https://doi.org/10.1142/S0217751X19420144.

[14] J. Grames *et al.*, "High precision 5 MeV Mott polarimeter", *Phys. Rev. C* , 102, 015501 (2020); https://doi.org/10.1103/PhysRevC.102.015501.

[15] G. Palacios-Serrano *et al.*, "High voltage design and evaluation of Wien filters for the CEBAF 200 keV injector upgrade", *International Particle Accelerator Conference, IPAC 2021* ; https://doi.org/10.18429/JACoW-IPAC2021-MOPAB324.

[16] V. Tioukine *et al.*, "Operation of the MAMI accelerator with a Wien filter based spin rotation system", *Nuclear Instruments and Methods in Physics Research Section A* 568, Pages 537-542; https://doi.org/10.1016/j.nima.2006.08.022.